SCIENCE CHINA
Earth Sciences

•RESEARCH PAPER•

https://doi.org/10.1007/s11430-017-9209-9

Crustal azimuthal anisotropy in the trans-North China orogen and adjacent regions from receiver functions

Yan YANG[1], Huajian YAO[1,2*], Ping ZHANG[1] & Ling CHEN[3]

[1]*Laboratory of Seismology and Physics of Earth's Interior and School of Earth and Space Sciences, University of Science and Technology of China, Hefei 230026, China;*
[2]*Mengcheng National Geophysical Observatory, University of Science and Technology of China, Mengcheng 233500, China;*
[3]*Institute of Geology and Geophysics, Chinese Academy of Sciences, Beijing 100029, China*

Received October 10, 2017; revised February 23, 2018; accepted April 19, 2018; published online May 24, 2018

Abstract The North China Craton (NCC) is an important part of eastern China. Recent studies have shown that the eastern NCC (ENCC) has undergone significant lithospheric thinning and destruction since the late Mesozoic. Destruction of the cratonic lithosphere is necessarily accompanied by crustal deformation. Therefore, a detailed crustal deformation model can provide basic observational constraints for understanding the process and mechanisms of the destruction of the NCC. In this study, we estimated the crustal azimuthal anisotropy beneath 198 broadband stations in the NCC with a joint analysis of Ps waves converted at the Moho from radial and transverse receiver function data. We also performed a harmonic analysis to test the reliability of the measured anisotropy. We obtained robust crustal azimuthal anisotropy beneath 23 stations that are mostly located on the western margin of the Bohai Bay Basin, Yin-Yan orogenic belt, and Taihang Mountains, which reflects the crustal deformation characteristics in those regions. The crustal shear wave splitting time was found to range from 0.05 s to 0.68 s, with an average value of 0.23 s, which reveals a distinct crustal anisotropy in the Trans-North China Orogen (TNCO) and its adjacent areas. Our analysis of the results suggests that the strong NW-SE tectonic extension in the late Mesozoic and Cenozoic played an important role in crustal anisotropy in this region. In addition, the E-W trending crustal anisotropy on the margin of the Bohai Bay Basin indicates an effect of the ENE-WSW trending horizontal principal compressive stress. The crustal anisotropy in the Yin-Yan orogenic belt may be an imprint of the multiple-phase shortening of a dominant N-S direction from the early-to-middle Jurassic to the Early Cretaceous. Stations in the Taihang Mountains show large splitting times and well-aligned NW-SE fast directions that correlate with those measured from SKS splitting and that are possibly related to the lithospheric modification and magmatic underplating from the Late Mesozoic to Cenozoic in this area.

Keywords North China Craton, Receiver Functions, Crust, Azimuthal Anisotropy

Citation: Yang Y, Yao H, Zhang P, Chen L. 2018. Crustal azimuthal anisotropy in the trans-North China orogen and adjacent regions from receiver functions. Science China Earth Sciences, 61, https://doi.org/10.1007/s11430-017-9209-9

1. Introduction

The North China Craton (NCC) in eastern China, which is the largest and oldest craton in China, is mainly composed of three parts: the western NCC (WNCC), the Trans-North China Orogen (TNCO), and the eastern NCC (ENCC) (Zhao et al., 2001, 2005). The NCC has undergone intense lithospheric thinning since the Mesozoic, during which the ancient, thick (~200 km), and refractory cratonic lithospheric mantle of the ENCC was replaced by the younger, thinner (<100 km), and relatively fertile oceanic lithospheric mantle in concert with large-scale tectonic deformation, magmatic activity, and the formation of extensional basins (Menzies et al., 1993; Griffin et al., 1998; Xu Y G, 2001; Wu et al., 2005;

* Corresponding author (email: hjyao@ustc.edu.cn)

Chen, 2010; Zhu et al., 2011). By contrast, most parts of the WNCC maintained stable cratonic properties, including few magmatic activities and low surface heat flux (Hu et al., 2000). The N-S trending TNCO was formed by the collision of the eastern and western blocks approximately 1.85 billion years ago, marking the notable variations in surface topography, gravity anomaly, and lithosphere thickness (Zhao et al., 2001, 2005; Zhu et al., 2011). Therefore, it is an ideal location to study the variation styles of lithospheric properties. The study region consists of three major tectonic units: the Bohai Bay Basin in the east, the Yin-Yan orogenic belt in the north, and the Taihang Mountains in the middle (Figure 1). The Yin-Yan orogenic belt underwent multiple phases of N-S directed contraction from the early-to-middle Jurassic to the Early Cretaceous, which was followed by large-scale E-W tectonic extension and magmatic activities (Davis et al., 2001; Zheng et al., 2000).During the late Early Cretaceous, with the abrupt change in the subduction direction of the paleo-Pacific plate that led to the backarc extension in the shallow crust, eastern China experienced intense NW-SE trending extension. The subsidence of the Bohai Bay Basin and the uplift of the Taihang Mountains are often considered to be related to the NW-SE extension during that period (Xu Y G, 2001; Ren et al., 2002; Zheng et al., 2008; Zhu et al., 2012).

Tectonic deformation can produce anisotropy at a seismic wavelength scale (Mainprice and Nicolas, 1989), and seismic anisotropy therefore provides an effective tool to study the deformation and evolution of the lithosphere. Anisotropy in the upper crust can be divided into two categories: stress-induced anisotropy resulting from water-saturated microcracks and structural anisotropy due to fault zones and sedimentary bedding planes (Crampin et al., 2003; Boness and Zoback, 2006). However, anisotropy in the lower crust to upper mantle is often interpreted as the preferred orientation of minerals, or lattice preferred orientation (LPO) (Silver, 1996). Shear wave splitting (SWS) is one of the most commonly-used techniques for estimating azimuthal anisotropy, for which two parameters of interest are the fast shear wave polarization direction and delay time. The fast direction reveals the direction of the symmetry axis of the anisotropic medium, whereas the delay time depends on the strength of anisotropy and the length of the propagation path of the shear wave in the anisotropic medium (Bowman and Ando, 1987; Silver and Chan, 1991). This technique has been widely adopted to study crustal and mantle anisotropy in the NCC in previous work. Zhao and Zheng (2005) found a distinct difference between fast polarization directions measured from SKS in the TNCO and ENCC and proposed a corresponding asthenospheric flow model. Gao et al. (2010) found that fast polarization directions measured from local S-waves and teleseismic SKS waves are inconsistent, suggesting that the crust and the upper mantle are not simply coupled in this region. SKS results from Chang et al. (2012) indicated a good correlation between the fast direction of upper mantle anisotropy and the absolute plate motion in the NCC. The fast direction of upper mantle anisotropy from their results in the TNCO shows little discrepancy with that in the ENCC and WNCC. The SWS measured from local data can reflect seismic anisotropy in the upper-middle crust. The SKS splitting tends to be attributed to the contribution of the upper mantle, usually neglecting crustal anisotropy (Vinnik et al., 1984, 1989; Silver and Chan, 1991). However, modeling

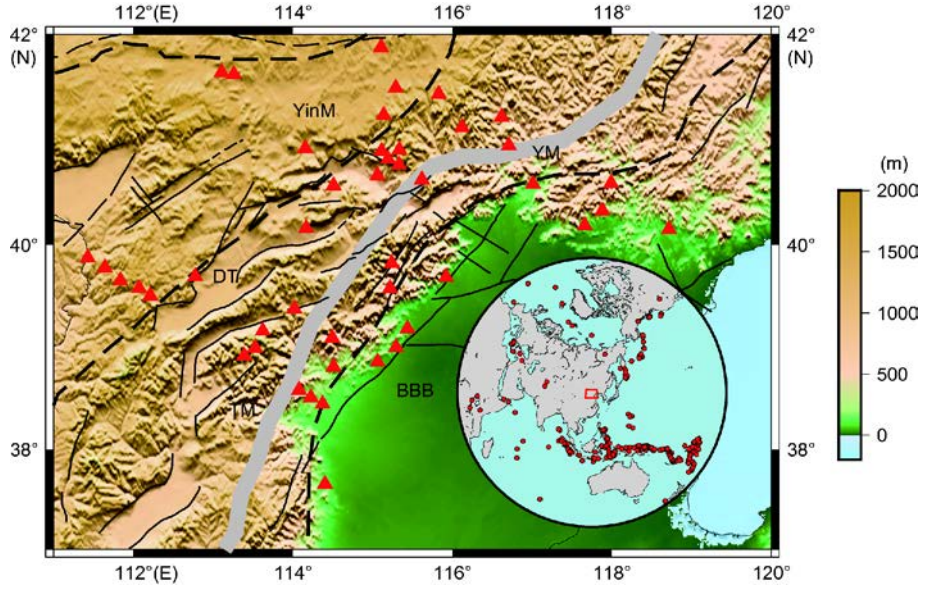

Figure 1 Topography and tectonic settings of the study region. The background color maps the topography (unit: m). The red triangles represent the selected 45 stations. The solid thin black lines represent faults. The bold grey line represents the North-South Gravity Lineament (NSGL). The dashed black lines represent boundaries between the western NCC, the TNCO, and the eastern NCC. The inset shows the location of the study region and the distribution of teleseismic events. YinM: Yin Mountains, YM: Yan Mountains, TM: Taihang Mountains, BBB: Bohai Bay Basin, DT: Datong Basin.

undertaken by Ruan et al. (2004) showed that in some cases such as when the direction of the symmetry axis of the crustal anisotropy is parallel with or perpendicular to that of the mantle anisotropy, the presence of crustal anisotropy could have a considerable effect on SKS splitting results. Therefore, we believe that the azimuthal anisotropy of the whole crust, combined with the SWS results from local seismic data and SKS, can help us better understand the deformation of the crust and mantle at different depths.

In recent years, SWS has been applied to the Moho converted Ps waves of receiver functions and has aided in finding significant crustal anisotropy (e.g., McNamara and Owens, 1993; McNamara et al., 1994; Nagaya et al., 2008). To improve the stability and reliability for estimating crustal anisotropy, Liu and Niu (2012) developed a technique with a joint analysis of radial and transverse receiver function data. This technique has been successfully performed to study the crustal deformations beneath the SE Tibetan Plateau (Sun et al., 2012) and the NE margin of the Tibetan Plateau (Wang et al., 2015). Sun et al. (2012) found that significant crustal anisotropy exists beneath some stations in the southeastern margin of the Tibetan Plateau, which may be the major contributor to the teleseismic SWS. Chen et al. (2013) claimed a decoupled deformation pattern between the crust and upper mantle beneath Yunnan based on the obvious differences in fast directions obtained from the splitting of the Moho Ps wave and SKS. Wu et al. (2015) used the teleseismic XKS phases (PKS, SKS, and SKKS phases) to detect the presence of double-layer crustal anisotropy in western Tibet. They found that the splitting parameters of the upper layer are consistent with those measured from Moho converted Ps phases, suggesting an NE-SW trending crustal anisotropy that may be related to plastic flow in the middle to lower crust.

To further understand the crustal deformation and the crust-mantle coupling mechanism of the TNCO and its adjacent regions, we adopted the technique from Liu and Niu (2012) and a harmonic analysis (Sun et al., 2012) to obtain reliable crustal average azimuthal anisotropy. We also discuss the spatial variation and the generation mechanism of crustal anisotropy in this region.

2. Data and methods

2.1 Data processing

The Institute of Geophysics of the China Earthquake Administration deployed the North China Seismic Array (ChinArray, 2006) in the northeastern NCC from 2006 to 2009, which was composed of 250 temporary stations in the region of 37°−42°N, 111°−120°E, to study the fine structure of the crust and upper mantle in that area. We selected 322 teleseismic events recorded at 198 broadband stations with magnitudes greater than 5 and epicentral distances within 30°−90°, most of which had back azimuths in the range of 110°−240° (Figure 1).

The raw data were cut according to the P wave arrival time calculated with the IASP91 model (Kennett and Engdahl, 1991), resampled to 10 Hz and band-pass filtered in a frequency band of [0.1, 1] Hz. We then eliminated those waveforms with unrecognized P-wave phases or low signal-noise-ratios (SNRs). We used the time domain deconvolution method (Ammon, 1991) to extract receiver functions, for which the Gaussian parameter was set to 2.5. Finally, we obtained more than 20000 receiver function traces. To obtain more reliable anisotropy results, we visually inspected the radial receiver function waveforms from all 198 stations and selected only 45 stations situated on bedrock with clear Moho Ps converted phases and relatively good back azimuthal coverage (Figure 1). Those stations were distributed in the TNCO and its adjacent areas but barely covered the eastern NCC due to the influence of thick sedimentary basins.

Because our study of crustal anisotropy is based on the variation of Ps phase arrival time with back azimuth, we needed to first remove the effects due to different ray parameters. According to the H-κ results from Wu (2011) and the Preliminary Reference Earth Model (PREM) of Dziewonski and Anderson (1981), we computed the moveout and make corrections to a standard epicentral distance of 60° and a source depth of 0 km (ray parameter about 6.8 s/(°)). To improve the SNR, we further stacked the receiver functions every 5° in back azimuth and manually picked the time window of the Ps phase (Figure 2).

2.2 Estimating crustal anisotropy with receiver function gathers

When a radially polarized shear wave is incident to an isotropic medium, the energy is concentrated in the radial direction, and nearly no energy appears on the transverse component. By contrast, a shear wave passing through an anisotropic crust with a horizontal axis of symmetry will split into two shear waves with nearly orthogonal polarizations and different speeds. A clear 180°-periodicity variation in the Ps arrival times on the radial component and the polarity of the Ps phase on the transverse component can be observed from receiver functions, which is a feature that is distinguishable from other crustal heterogeneities.

Traditional methods used to estimate crustal anisotropy with receiver functions are single-event based (McNamara and Owens, 1993; McNamara et al., 1994; Nagaya et al., 2008), which is the same as techniques developed for SKS splitting analysis, and take results from the average of all measurements. We applied the method based on a joint analysis of receiver function gathers developed by Liu and

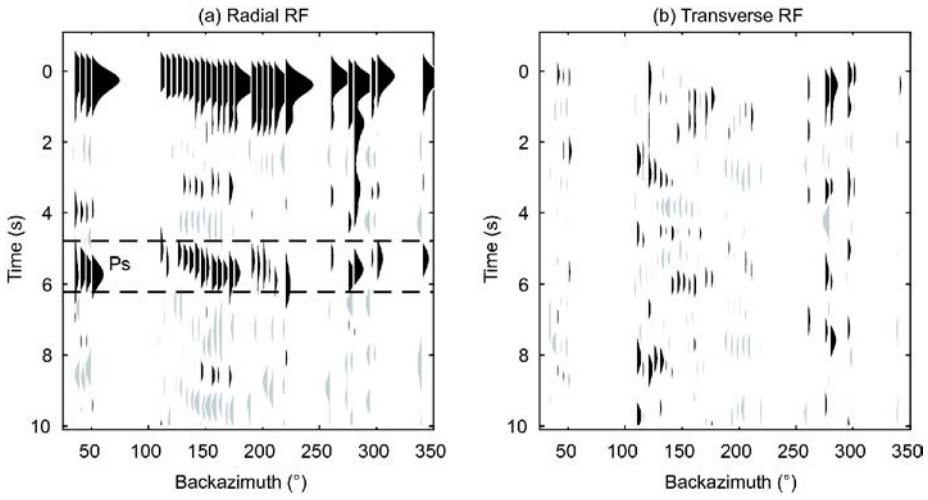

Figure 2 Receiver functions recorded at station A106. Radial (a) and transverse (b) receiver functions recorded at station A106 are plotted as a function of back azimuth (stacked each 5°). The dashed lines in (a) delineate the time window of the Ps phase arrivals, which apparently varied with back azimuth.

Niu (2012). They used the receiver function gathers and managed to find one pair of splitting parameters (φ, δt) (i.e., fast wave direction, fast and slow wave splitting time) that fits all the receiver functions collected at a station. Their method includes computing three individual objective functions (IOF) and a joint objective function (JOF). The three IOFs aim to search for a pair of best-fit splitting parameters to (1) maximize the radial peak energy I_{rcos} with a cosine moveout correction, (2) maximize the radial correlation coefficient I_{rcc} after removing anisotropy, and (3) minimize the transverse energy I_t after removing anisotropy. The JOF can be computed with the three IOFs by the following formula:

$$I(\varphi,\delta t)=\frac{I_{rcos}(\varphi,\delta t)I_{rcc}(\varphi,\delta t)}{I_t(\varphi,\delta t)}. \quad (1)$$

More details about this method can be found in Liu and Niu (2012).

Figure 3 shows our grid search results at station A801 obtained with this method. The objective functions were computed in a range of (0−360°, 0−1.2 s) with increments of (1°, 0.01 s). Three IOFs and the JOF are shown in Figures 3a, b, c and Figure 3d, respectively. For better visualization, we plotted the inverse of I_t. The fast direction (red region, with the maximum value of the objective function) is quite consistent in each subplot (Figure 3a, b, c). The JOF in Figure 3d displays a best-fitted pair of fast direction and splitting time. Figures 4a and 4b plot the original receiver functions at this station and the waveforms after removing anisotropy with the best-fitted pair of splitting parameters, respectively. We also forward modeled the receiver functions at this station with an isotropic crustal model from Wu (2011), adding the crustal anisotropy computed from our search results. The predicted Ps arrival times (red dots in Figure 4a) at different back azimuths fit the observed data well. Figure 4c plots the stacked waveforms before and after anisotropy removal, and the stacked Ps phase energy is apparently higher than that of the original stacked waveform, suggesting the existence of crustal azimuthal anisotropy.

2.3 Harmonic analysis

Other than S-wave azimuthal anisotropy, there are several factors that can affect the Ps phase arrival time, such as a dipping Moho, P-wave anisotropy, and some small-scale lateral variations in the crust, etc. Previous studies have demonstrated that different types of crustal structures tend to result in different harmonic degrees in back azimuth variations in Ps arrival times (Kosarev et al., 1984; Levin and Park, 1997; Savage, 1998; Bianchi et al., 2010). A dipping Moho, P-wave anisotropy, and S-wave anisotropy with a tilted axis of symmetry have degree-1 back azimuth variations. S-wave azimuthal anisotropy has a degree-2 back azimuthal variation. Crustal structures with smaller-scale heterogeneity (such as micro cracks) usually lead to higher-order harmonic variations. A previous modeling (Wang et al., 2016) also suggests that the presence of a dipping Moho causes a considerable perturbation on the strength of estimated crustal anisotropy. To avoid these interference factors and determine whether the Ps arrival time variations resulted from S-wave azimuthal anisotropy, we performed a harmonic analysis developed from Sun et al. (2012). The method includes correcting receiver functions with different assumed harmonic degrees and calculating the maximum amplitude and the maximum energy of stacked receiver functions after correction. Then we can judge whether the Ps arrival time variations are mainly contributed from azimuthal anisotropy.

Figure 5 shows the results of the harmonic analysis performed at station A801. The maximum amplitude and the maximum energy of the corrected and stacked receiver

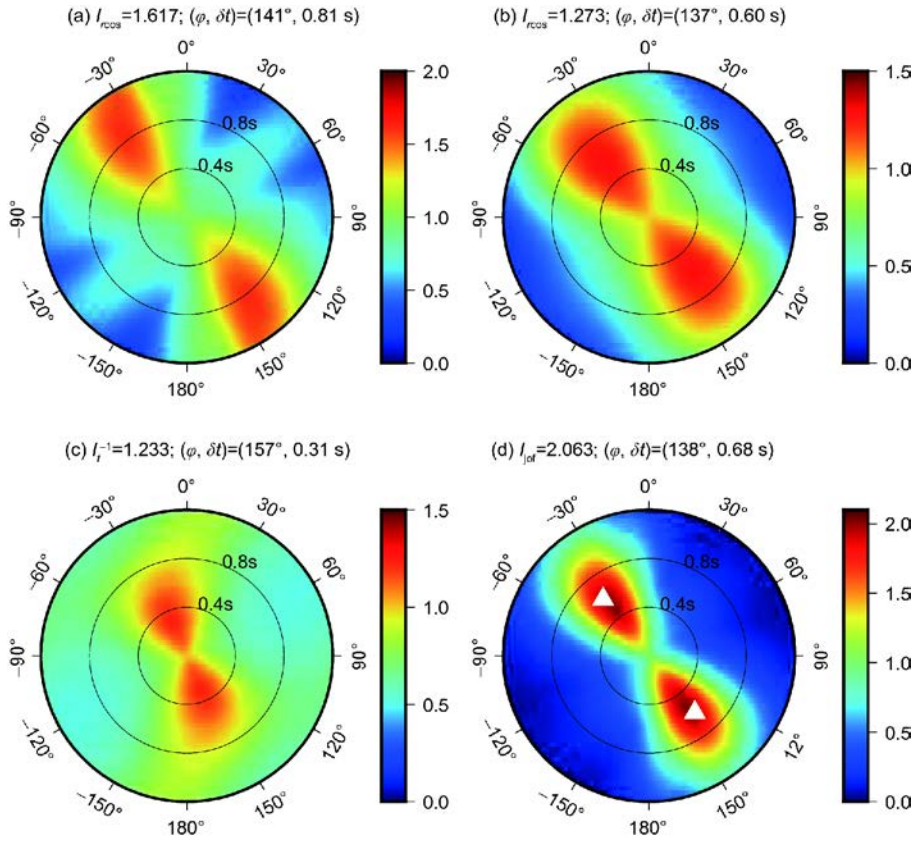

Figure 3 Crustal anisotropy estimation at station A801. (a) Radial peak energy I_{rcos} in the Ps arrival time window with cosine moveout correction, (b) radial correlation coefficient I_{rcc} in the Ps arrival time window after removing anisotropy, (c) inverse of transverse energy I_t in the Ps arrival time window after removing anisotropy, (d) averaged JOF. The white triangles denote a fast wave direction of 138° and a splitting time of 0.68 s corresponding to the maximum JOF. Azimuth and radius represent fast wave direction and splitting time, respectively. The objective functions were searched in a range of (0−360°, 0−1.2 s) with increments of (1°, 0.01 s).

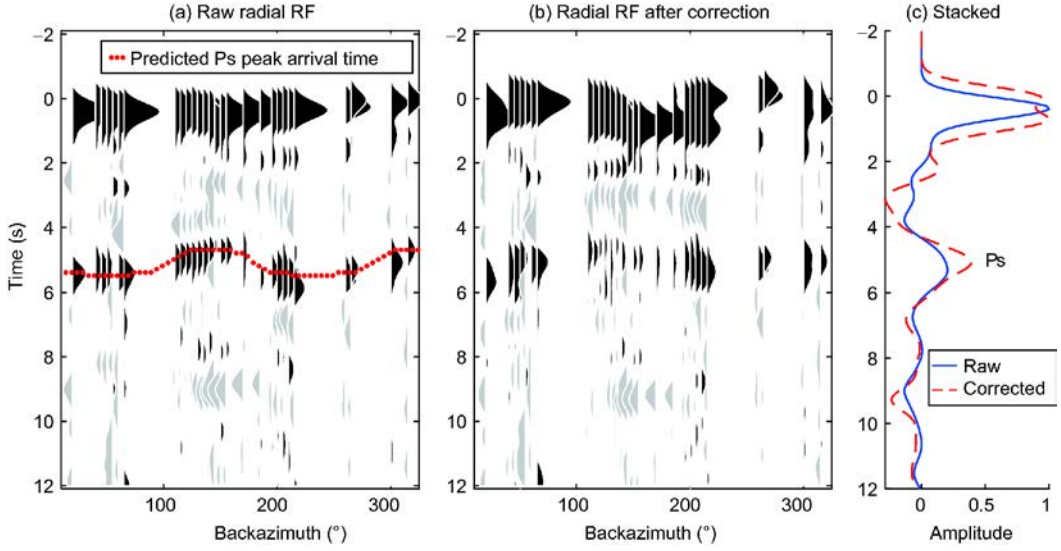

Figure 4 Comparison of radial RFs before and after anisotropy removal at station A801. (a) Original receiver functions, (b) waveforms after removing crustal anisotropy with the best-fitted pair of splitting parameters, (c) stack of waveforms in (a) and (b). The red dots in (a) denote the predicted Ps arrival times computed from the assumed anisotropy at different back azimuths. The blue line and the red line are the stacked waveforms before and after anisotropy removal, respectively.

functions reach a peak at degree-2, indicating that the S-wave azimuthal anisotropy is a major contributor to splitting parameters rather than other heterogeneous crustal structures.

2.4 Statistical error estimation

SNR-based reliability analyses are commonly used to testify the estimated anisotropy (Liu and Niu, 2012; Sun et al., 2012; Wang et al., 2015). However, we cannot obtain the noise level before P arrival time because we adopted the time domain deconvolution when extracting the receiver functions. Instead, we used a statistical bootstrap approach to estimate the error of our results. We randomly resampled the same number of receiver functions as before (although one receiver function could be resampled less or more than once) under a single station to generate new receiver function gathers. The new receiver function gathers were again stacked at every 5° back azimuth, and the same method for anisotropy estimation was applied. This process was repeated 50 times to generate a distribution of splitting parameters, from which we calculated the mean values and standard errors.

Figure 6 shows the distributions of the statistical results at station A801. The search results from the original receiver function gathers were close to the mean value of resampled bootstrap results. The fast direction differed by less than 2°, and the splitting time differed by less than 0.02 s, indicating the stability of the results from this method.

3. Results

After performing the harmonic analysis on receiver functions at all 45 stations, we eliminated some stations with apparent harmonic orders of 1 that are probably affected by the dipping Moho (Wang et al., 2016). Twenty-three of the stations exhibit strong degree-2 harmonic orders, indicating that the measured splitting results mainly arise from azimuthal anisotropy. The splitting parameters are listed in Table 1, and the 95% confidence interval is given by the standard errors from the bootstrap approach.

The measured splitting times with an average value of 0.23 s and a maximum of 0.68 s indicate distinct crustal azimuthal anisotropy in the TNCO and its adjacent regions. Figure 7 displays our crustal anisotropy results in this region, the strengths and directions of which are quite diverse. We ascribe the difference in anisotropy to the complexity and spatial variations in crustal deformation since this region has undergone several different periods of deformation. In addition, based on a single-layer crustal anisotropy hypothesis in our study, multi-layer anisotropy may exhibit a very small splitting time in an averaged apparent anisotropy, which may be misinterpreted as weak anisotropy. The upper mantle anisotropy from SKS splitting (Chang et al., 2012), the direction of the maximum horizontal compressive stress, and the absolute plate motion are plotted in Figure 7 as well. Considering the strength and direction of the measured

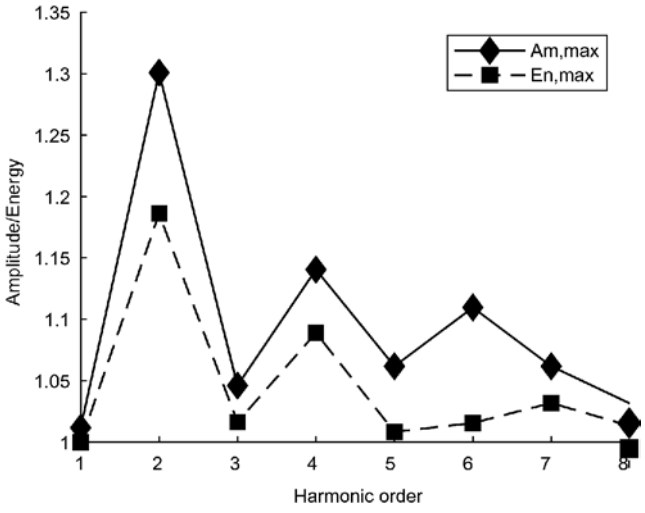

Figure 5 Results of the harmonic analysis at station A801. The solid and dashed lines represent the maximum amplitude and the maximum energy of the stacked Ps phase after assuming different harmonic degrees, respectively.

crustal anisotropy and tectonic settings in this region, we roughly divided the stations into three categories (Figure 7): stations in the margin of the Bohai Bay Basin with nearly E-W fast directions and small splitting times, stations in the Yin-Yan orogenic belt with NW-SE fast directions and increasing splitting times from north to south, and stations in the Taihang Mountains and other regions in the TNCO with strong anisotropy of NW-SE fast direction that are well correlated with the SKS results.

4. Discussion

4.1 Crustal anisotropy in the margin of the Bohai Bay Basin

Stations VZAH, A909, ZHKD, ZUNH and A406, which are situated on the boundary of the Taihang Uplift and the Bohai Bay Basin in the eastern NCC (Figure 7), display relatively small splitting times about 0.2 s and E-W fast directions in agreement with the N86°E fast wave direction measured from local seismic events (Gao et al., 2011). According to analyses from fault kinematics, sedimentology, and petrology, the abrupt change in the direction of the subduction of the Pacific plate during the late Early Cretaceous controlled the back arc extension direction of continental margin, which led to the intense NW-SE trending extension in the ENCC (Xu Y G, 2001; Ren et al., 2002; Zhu et al., 2012). According to earthquake source and borehole data, the direction of the maximum horizontal compressive stress in the NCC is N71.6°E (Xu Z H, 2001). Therefore, we speculate that the nearly E-W trending fast direction on the margin of the Bohai Bay Basin may be a result of the collective effect of the NW-SE crustal extensional deformation in the Early

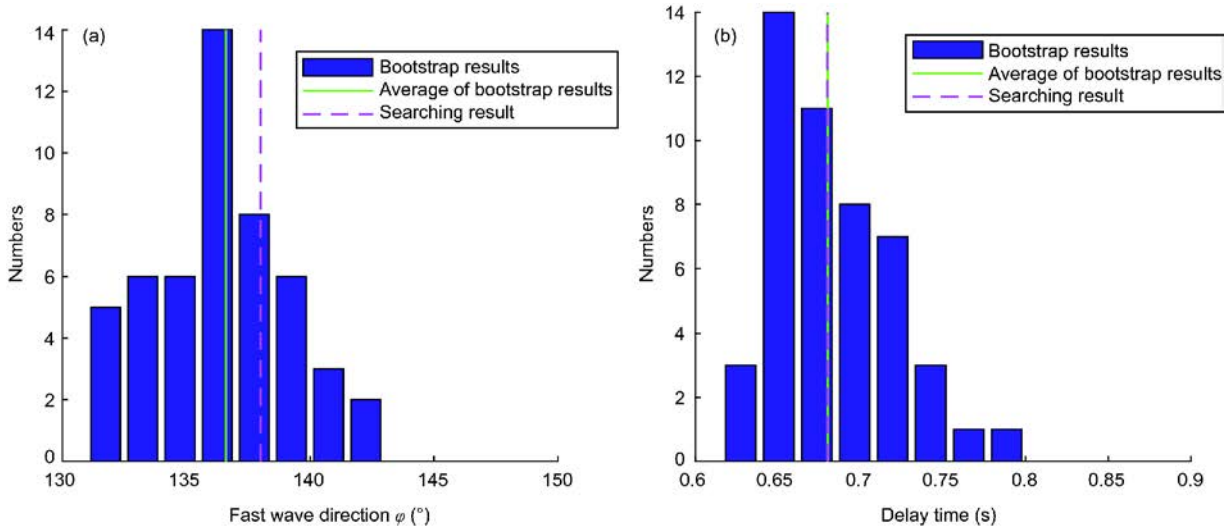

Figure 6 Histograms of the statistics of the azimuth anisotropy parameters at station A801. (a) Distributions of fast wave direction; (b) distributions of splitting time. The red lines denote the search results from the original receiver function gathers, and the green lines denote the average results from the bootstrap approach.

Table 1 Crustal anisotropy parameters in TNCO and its adjacent regions

Station	Latitude (°N)	Longitude (°E)	$\varphi\pm\Delta\varphi$ (°)	$\delta t\pm\Delta\delta t$ (s)	Number of events
A103	41.2	115.1	123±4	0.3±0.08	142
A105	41.5	115.3	118±10	0.05±0.02	108
A106	40.9	115.3	120±2	0.29±0.03	203
A110	41.4	115.8	134±8	0.13±0.05	158
A202	41.1	116.1	88±3	0.16±0.03	173
A406	40.2	118.7	67±8	0.15±0.03	198
A504	40.9	114.2	156±7	0.11±0.03	126
A507	40.6	114.5	123±2	0.33±0.04	185
A603	39.8	115.2	121±4	0.24±0.03	213
A801	39.7	112.8	138±3	0.68±0.04	143
A806	39.0	113.5	132±3	0.27±0.05	137
A807	39.2	113.6	134±5	0.31±0.05	142
A904	39.1	114.5	112±3	0.41±0.09	102
A909	39.2	115.4	88±2	0.23±0.02	179
K001	41.6	113.1	84±5	0.33±0.06	145
K018	40.9	115.1	135±4	0.27±0.07	150
K020	40.8	115.3	116±2	0.41±0.05	169
K022	40.6	115.6	115±4	0.31±0.04	193
VFEN	41.2	116.6	112±11	0.06±0.03	230
VLIQ	39.4	114.0	150±7	0.16±0.05	202
VZAH	37.7	114.4	154±6	0.07±0.03	239
ZHKD	39.7	115.9	78±19	0.05±0.02	227
ZUNH	40.2	117.7	88±2	0.23±0.02	179

Cretaceous and the current ENE-WSW maximum horizontal compressive stress in the crust.

Although the splitting times at stations ZHKD and VZAH are as small as 0.05 s, the recorded Ps phases show clear degree-2 harmonic order. We suggest that the crustal anisotropy may vary with depth such as the orthogonal fast direction in the upper and lower crust, which leads to a relatively small averaged anisotropy with a one-layer anisotropy hypothesis.

In contrast to those in other regions in the TNCO, crustal

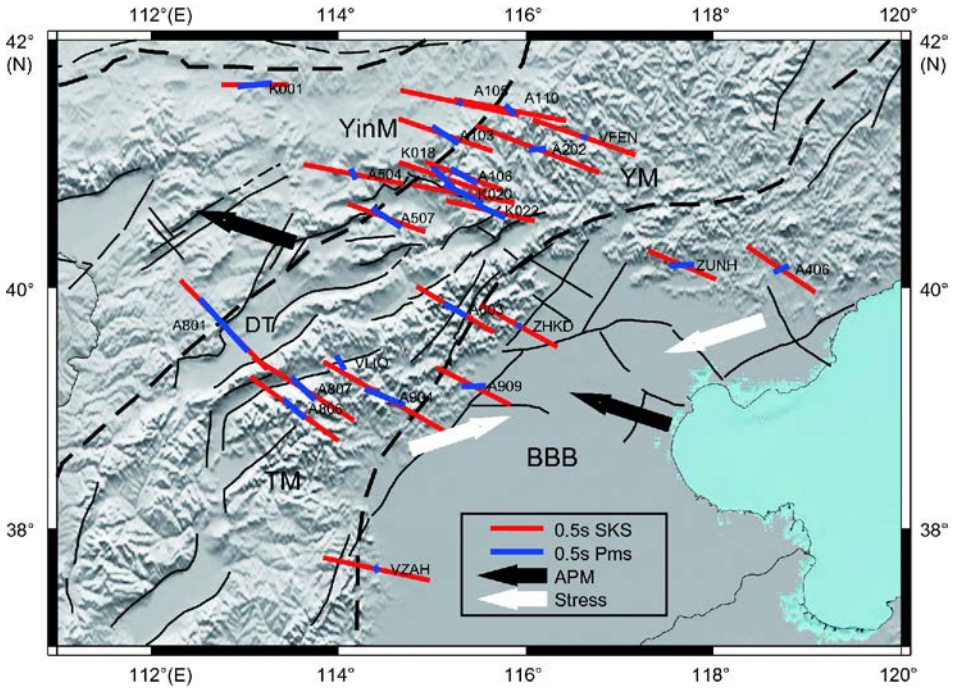

Figure 7 Crustal anisotropy in the TNCO and its adjacent regions. The background labels are the same as those in Figure 1. The blue and red bars represent the crustal anisotropy from the Moho Ps phase in this study and the upper mantle anisotropy from the SKS results (Chang et al., 2012), respectively. The lengths of the bars represent the splitting times, and the azimuths of the bars represent fast wave direction. The black arrows denote the N288°E absolute plate motion direction (Gripp and Gordon, 2002). The white arrows denote the N71.6°E maximum horizontal compressive stress field in the NCC (Xu Z H, 2001).

anisotropy on the margin of the Bohai Bay Basin is not correlated with the upper mantle anisotropy measured from SKS (Chang et al., 2012). The SKS results display fast directions similar to the absolute plate motion (WNW-ESE), thus manifesting the dominant role played by the current mantle flow. On the other hand, crustal anisotropy in this region is affected by the current maximum horizontal compressive stress, which results in differences in the observed crustal and mantle anisotropy. Moreover, these stations are on the boundary of the uplift and basins as well as the boundary of two regions with orthogonal lithospheric extension (Zhao et al., 2008), where complex crustal deformation probably occurred, thus affecting the results of average crustal azimuthal anisotropy.

4.2 Crustal anisotropy in the Yin-Yan orogenic belt

Stations situated in the Yin-Yan orogenic belt (Figure 7) such as A106, K018, K020 and K022 display moderate splitting times of approximate 0.3 s and well-aligned NW-SE fast directions, which can be best interpreted as the consequence of the widespread NW-SE trending extension in the Early Mesozoic (Xu Y G, 2001; Ren et al., 2002; Zhu et al., 2012).

Stations A105, A110, and VFEN in the northern part of the study region display smaller splitting times and nearly E-W trending fast directions. Field studies and regional volcanic rocks reveal multiple phases of folding and N-S trending contraction in the Yan Mountains from the Jurassic to Early Cretaceous (Davis et al., 2001; Zheng et al., 2000). The crust beneath these stations may have undergone this N-S trending contraction as well as the NW-SE extension, resulting in complex crustal anisotropy, from which we can only observe a relatively small apparent splitting time. Station K001 in the Yin Mountains in the western NCC, northwest of the study region, however, displays a splitting time exceeding 0.3 s and an E-W trending fast direction that is subparallel to the SKS results (Figure 7). Contrary to the eastern NCC, the western NCC is thought to be hardly affected by the NW-SE extensional deformation. The major source of crustal anisotropy was supposed to be the multiple phases of N-S trending contraction from the Jurassic to Early Cretaceous. As a result, the fast directions of the crust and lithosphere are subparallel to the trend of the orogen.

4.3 Crustal anisotropy in the Taihang Mountains

Other stations such as A806, A904, A507, and A603 are mostly situated in the Taihang Mountains and A801 is near the Datong Basin. These stations generally have large splitting times and NW-SE trending fast directions that are well aligned with the SKS results. Chang et al. (2012) attributed the SKS results to upper mantle anisotropy controlled by present-day mantle flow parallel to the absolute plate motion. Nevertheless, the fast directions at some stations do not quite

agree with the direction of the relatively slow absolute plate motion (Figure 7), which is also insufficient to explain the apparent SKS splitting time. Combining our results with the large splitting time and fast direction in the crust parallel to the SKS splitting results, we conclude that the crustal anisotropy in this region is non-negligible in the SKS results. Receiver function imaging detects thick crust-mantle boundary zones beneath the Taihang Mountains (Zhang et al., 2018). Surface wave tomography reveals low seismic velocity anomalies in the middle to lower crust and upper mantle in this region (Jiang et al., 2013; Zhang et al., 2018). There is other evidence, in particular high-conductivity anomalies (Zhang et al., 2016), high surface heat flow (Hu et al., 2000; Guo et al., 2016), and voluminous magmatic activities together with underplating (Chen et al., 2001; Xu et al., 2005; Li et al., 2013) in the Mesozoic to the Cenozoic. All of the above suggest that the lithospheric thinning and modification resulted from the intense NW-SE trending tectonic extension in this region. Given these facts, we propose that the crustal anisotropy and deformation in the Taihang Mountains is significantly affected by the extension that occurred in the Late Mesozoic and further affected by lithospheric modification since the Cenozoic.

Station A801 near the Datong Basin displays a dramatically large splitting time of 0.68 s and a fast direction that is slightly different from those of the other stations, which may be related to the more intense underplating due to the basaltic magmatic activities around the Datong Basin during the Quaternary (Zheng et al., 2008; Chen et al., 2001). This will result in stronger anisotropy in the lower crust.

4.4 Discussion of the methods used for seismic anisotropy analysis

Seismic anisotropy can be obtained from different observations including shear wave splitting data, surface wave dispersion curves, and receiver functions. Commonly-used phases in shear wave splitting are SKS (SKKS) waves, Moho Ps converted waves, and local S-waves. SKS results reflect the integrated effect of azimuthal anisotropy along the ray path from the core mantle boundary to a station, whereas Moho Ps converted waves and local S-waves provide constraints on the whole crust below and the path across the upper to middle crust, respectively (e.g., Vinnik et al., 1984, 1989; Silver and Chan, 1991). However, there is lack of vertical resolution in the shear wave splitting method due to the trade-offs between the strength of anisotropy and the length of the anisotropic ray path. Receiver functions are sensitive to the velocity interface and have the potential of resolving multi-layer anisotropy (e.g., Savage, 1998; Farra and Vinnik, 2000; Frederiksen and Bostock, 2000). Surface wave dispersions provide constraints on both azimuthal and radial anisotropy and with a better vertical resolution, yet horizontal resolution is limited due to their long periods and wavelengths (e.g., Yao et al., 2010; Lin et al., 2011; Xie et al., 2015). Our study employing measurements from Moho Ps receiver functions provides the average azimuthal anisotropy of the whole crust. However, the anisotropy below some stations may vary over depth, resulting in a small apparent average anisotropy and an unrecognized fast direction. Our future work will focus on a joint inversion with multiple data types to obtain better-resolved anisotropy in the crust and upper mantle.

5. Conclusions

Based on our crustal anisotropy results measured from Moho converted Ps phase and previous geophysical and geological work in the TNCO, we draw the following conclusions. Crustal deformation that resulted from the strong NW-SE tectonic extension in the late Mesozoic plays an important role in crustal azimuthal anisotropy in this region. The average splitting time of 0.2 s and the nearly E-W trending fast direction in the margin of the Bohai Bay Basin, consistent with local shear wave splitting data, may result from both the strong NW-SE trending tectonic extension and the present-day ENE-WSW trending horizontal principal compressive stress. The diverse splitting times (0.05–0.3 s) and NW-SE to E-W trending fast directions in the Yin-Yan orogenic belt may be an imprint of the multiple phases of N-S trending shortening from the Jurassic to Early Cretaceous. The large splitting time and NW-SE trending fast direction that are well aligned with the SKS results in the Taihang Mountains indicate strong crustal anisotropy that is possibly related to the lithospheric modification and magmatic underplating from the Late Mesozoic to the Cenozoic in this region.

Acknowledgements *We thank the China Seismic Array Data Management Center at the Institute of Geophysics, China Earthquake Administration for providing waveform data for this study. We thank the two anonymous reviewers for their constructive comments and suggestions. This study was supported by the National Natural Science Foundation of China (Grant Nos. 41574034, 41688103, and 91414301).*

References

Ammon C J. 1991. Isolation of receiver effects from teleseismic P waveforms. Bull Seismol Soc Am, 81: 2504−2510

Bianchi I, Park J, Piana Agostinetti N, Levin V. 2010. Mapping seismic anisotropy using harmonic decomposition of receiver functions: An application to Northern Apennines, Italy. J Geophys Res, 115: 12317

Boness N L, Zoback M D. 2006. Mapping stress and structurally controlled crustal shear velocity anisotropy in California. Geology, 34: 825–828

Bowman J R, Ando M. 1987. Shear-wave splitting in the upper-mantle wedge above the Tonga subduction zone. Geophys J Int, 88: 25–41

Chang L J, Wang C Y, Ding Z F. 2012. Upper mantle anisotropy beneath North China (in Chinese). Chin J Geophys, 55: 886−896

Chen L. 2010. Concordant structural variations from the surface to the base of the upper mantle in the North China Craton and its tectonic implications. Lithos, 120: 96–115
Chen S, O'Reilly S Y, Zhou X, Griffin W L, Zhang G, Sun M, Feng J, Zhang M. 2001. Thermal and petrological structure of the lithosphere beneath Hannuoba, Sino-Korean Craton, China: evidence from xenoliths. Lithos, 56: 267–301
Chen Y, Zhang Z, Sun C, Badal J. 2013. Crustal anisotropy from Moho converted Ps wave splitting analysis and geodynamic implications beneath the eastern margin of Tibet and surrounding regions. Gondwana Res, 24: 946–957
ChinArray. 2006. China Seismic Array waveform data. China Earthquake Administration, doi: 10.12001/ChinArray.Data
Crampin S, Chastin S, Gao Y. 2003. Shear-wave splitting in a critical crust. J Appl Geophys, 54: 265–277
Davis G A, Zheng Y D, Wang C, Darby B J, Zhang C H, Gehrels G. 2001. Mesozoic tectonic evolution of the Yanshan fold and thrust belt with emphasis on Hebei and Liaoning provinces, northern China. Mem Geol Soc Am, 194: 171–197
Dziewonski A M, Anderson D L. 1981. Preliminary reference Earth model. Phys Earth Planet Inter, 25: 297–356
Farra V, Vinnik L. 2000. Upper mantle stratification by P and S receiver functions. Geophys J Int, 141: 699–712
Frederiksen A W, Bostock M G. 2000. Modelling teleseismic waves in dipping anisotropic structures. Geophys J Int, 141: 401–412
Gao Y, Wu J, Fukao Y, Shi Y, Zhu A. 2011. Shear wave splitting in the crust in North China: stress, faults and tectonic implications. Geophys J Int, 187: 642–654
Gao Y, Wu J, Yi G X, Shi Y T. 2010. Crust-mantle coupling in North China: Preliminary analysis from seismic anisotropy (in Chinese). Chin Sci Bull, 55: 2837−2843
Griffin W L, Andi Z, O'Reilly S Y, Ryan C G. 1998. Phanerozoic Evolution of the Lithosphere Beneath the Sino-Korean Craton. In: Flower M F J, Chung S L, Lo C H, eds. Mantle Dynamics and Plate Interactions in East Asia. Am Geophys Union, 27: 107−126
Gripp A E, Gordon R G. 2002. Young tracks of hotspots and current plate velocities. Geophys J Int, 150: 321–361
Guo Z, Chen Y J, Ning J, Yang Y, Afonso J C, Tang Y. 2016. Seismic evidence of on-going sublithosphere upper mantle convection for intraplate volcanism in Northeast China. Earth Planet Sci Lett, 433: 31–43
Hu S, He L, Wang J. 2000. Heat flow in the continental area of China: a new data set. Earth Planet Sci Lett, 179: 407–419
Jiang M, Ai Y, Chen L, Yang Y. 2013. Local modification of the lithosphere beneath the central and western North China Craton: 3-D constraints from Rayleigh wave tomography. Gondwana Res, 24: 849–864
Kennett B L N, Engdahl E R. 1991. Traveltimes for global earthquake location and phase identification. Geophys J Int, 105: 429–465
Kosarev G L, Makeyeva L I, Vinnik L P. 1984. Anisotropy of the mantle inferred from observations of P to S converted waves. Geophys J Int, 76: 209–220
Levin V, Park J. 1997. Crustal anisotropy in the Ural Mountains Foredeep from teleseismic receiver functions. Geophys Res Lett, 24: 1283–1286
Li S R, Santosh M, Zhang H F, Shen J F, Dong G C, Wang J Z, Zhang J Q. 2013. Inhomogeneous lithospheric thinning in the central North China Craton: Zircon U-Pb and S-He-Ar isotopic record from magmatism and metallogeny in the Taihang Mountains. Gondwana Res, 23: 141–160
Lin F C, Ritzwoller M H, Yang Y, Moschetti M P, Fouch M J. 2011. Complex and variable crustal and uppermost mantle seismic anisotropy in the western United States. Nat Geosci, 4: 55–61
Liu H, Niu F. 2012. Estimating crustal seismic anisotropy with a joint analysis of radial and transverse receiver function data. Geophys J Int, 188: 144–164
Mainprice D, Nicolas A. 1989. Development of shape and lattice preferred orientations: Application to the seismic anisotropy of the lower crust. J Struct Geol, 11: 175–189
McNamara D E, Owens T J, Silver P G, Wu F T. 1994. Shear wave anisotropy beneath the Tibetan Plateau. J Geophys Res, 99: 13655–13665
McNamara D E, Owens T J. 1993. Azimuthal shear wave velocity anisotropy in the Basin and Range Province using moho *Ps* converted phases. J Geophys Res, 98: 12003–12017
Menzies M A, Fan W, Zhang M. 1993. Palaeozoic and Cenozoic lithoprobes and the loss of >120 km of Archaean lithosphere, Sino-Korean craton, China. Geol Soc London Spec Publ, 76: 71–81
Nagaya M, Oda H, Akazawa H, Ishise M. 2008. Receiver functions of seismic waves in layered anisotropic media: Application to the estimate of seismic anisotropy. Bull Seismol Soc Am, 98: 2990–3006
Nu Z H. 2001. A present-day tectonic stress map for eastern Asia region (in Chinese). Earthquake Sci, 23: 492−501
Ren J, Tamaki K, Li S, Junxia Z. 2002. Late Mesozoic and Cenozoic rifting and its dynamic setting in Eastern China and adjacent areas. Tectonophysics, 344: 175–205
Ruan A G, Wang C Y, Li Q H, Zang H. 2004. Effect of the crust on the analysis of the upper mantle anisotropy (in Chinese). Chin J Geophys, 47: 441−448
Savage M K. 1998. Lower crustal anisotropy or dipping boundaries? Effects on receiver functions and a case study in New Zealand. J Geophys Res, 103: 15069–15087
Silver P G, Chan W W. 1991. Shear wave splitting and subcontinental mantle deformation. J Geophys Res, 96: 16429–16454
Silver P G. 1996. Seismic anisotropy beneath the continents: Probing the depths of geology. Annu Rev Earth Planet Sci, 24: 385–432
Sun Y, Niu F, Liu H, Chen Y, Liu J. 2012. Crustal structure and deformation of the SE Tibetan plateau revealed by receiver function data. Earth Planet Sci Lett, 349-350: 186–197
Vinnik L P, Farra V, Romanowicz B. 1989. Azimuthal anisotropy in the earth from observations of SKS at GEOSCOPE and NARS broadband stations. Bull Seismol Soc Am, 79: 1542−1558
Vinnik L P, Kosarev G L, Makeyeva L I. 1984. Anisotropy in the lithosphere from the observations of SKS and SKKS. Dok Acad Nauk SSSR, 278: 1335−1339
Wang Q, Gao Y, Niu F L, Chen Y T. 2016. Reliability analysis of crustal anisotropy from receiver functions and effect of dipping interface (in Chinese). Earthquake, 36: 14−25
Wang Q, Niu F, Gao Y, Chen Y. 2015. Crustal structure and deformation beneath the NE margin of the Tibetan plateau constrained by teleseismic receiver function data. Geophys J Int, 204: 167–179
Wu F Y, Lin J Q, Wilde S A, Zhang X, Yang J H. 2005. Nature and significance of the Early Cretaceous giant igneous event in eastern China. Earth Planet Sci Lett, 233: 103–119
Wu J, Zhang Z, Kong F, Yang B B, Yu Y, Liu K H, Gao S S. 2015. Complex seismic anisotropy beneath western Tibet and its geodynamic implications. Earth Planet Sci Lett, 413: 167–175
Wu Y. 2011. The structure of the crust and upper mantle in North China Craton from teleseismic receiver function (in Chinese). Doctral Dissertation. Institute of Geophysics, CEA
Xie J, Ritzwoller M H, Brownlee S J, Hacker B R. 2015. Inferring the oriented elastic tensor from surface wave observations: preliminary application across the western United States. Geophys J Int, 201: 996–1021
Xu Y G, Ma J L, Frey F A, Feigenson M D, Liu J F. 2005. Role of lithosphere–asthenosphere interaction in the genesis of Quaternary alkali and tholeiitic basalts from Datong, western North China Craton. Chem Geol, 224: 247–271
Xu Y G. 2001. Thermo-tectonic destruction of the archaean lithospheric keel beneath the sino-Korean Craton in China: Evidence, timing and mechanism. Phys Chem Earth Part A-Solid Earth Geodesy, 26: 747–757
Xu Z H. 2001. A present-day tectonic stress map for eastern Asia region (in Chinese). Acta Seismol Sin, 23: 492–501
Yao H, van der Hilst R D, Montagner J P. 2010. Heterogeneity and anisotropy of the lithosphere of SE Tibet from surface wave array tomography. J Geophys Res, 115: B12307
Zhang C, Yao H, Liu Q, Zhang P, Yuan Y O, Feng J, Fang L. 2018. Linear

array ambient noise adjoint tomography reveals intense crust-mantle interactions in North China Craton. J Geophys Res-Solid Earth, 123: 368–383
Zhang H, Huang Q, Zhao G, Guo Z, Chen Y J. 2016. Three-dimensional conductivity model of crust and uppermost mantle at the northern Trans North China Orogen: Evidence for a mantle source of Datong volcanoes. Earth Planet Sci Lett, 453: 182–192
Zhao G, Sun M, Wilde S A, Sanzhong L. 2005. Late Archean to Paleoproterozoic evolution of the North China Craton: Key issues revisited. Precambrian Res, 136: 177–202
Zhao G, Wilde S A, Cawood P A, Sun M. 2001. Archean blocks and their boundaries in the North China Craton: Lithological, geochemical, structural and *P-T* path constraints and tectonic evolution. Precambrian Res, 107: 45–73
Zhao L, Zheng T, Lü G. 2008. Insight into craton evolution: Constraints from shear wave splitting in the North China Craton. Phys Earth Planet Inter, 168: 153–162
Zhao L, Zheng T. 2005. Using shear wave splitting measurements to investigate the upper mantle anisotropy beneath the North China Craton: Distinct variation from east to west. Geophys Res Lett, 32: L10309
Zheng T Y, Zhao L, Zhu R X. 2008. Insight into the geodynamics of cratonic reactivation from seismic analysis of the crust-mantle boundary. Geophys Res Lett, 35: L08303
Zheng Y D, Davis G A, Wang C, Darby B J, Zhang C H. 2000. Major Mesozoic tectonic events in the Yanshan Belt and the plate tectonic setting (in Chinese). Acta Geol Sin, 74: 289−302
Zhu G, Jiang D, Zhang B, Chen Y. 2012. Destruction of the eastern North China Craton in a backarc setting: Evidence from crustal deformation kinematics. Gondwana Res, 22: 86–103
Zhu R X, Chen L, Wu F Y, Liu J L. 2011. Timing, scale and mechanism of the destruction of the North China Craton. Sci China Earth Sci, 54: 789–797

(Responsible editor: Yong ZHENG)